Search for high spin collective states in $^{12}C^* \rightarrow 3\alpha$

D.D. Caussyn, G.L. Gentry, J.A. Liendo, and N.R. Fletcher
Department of Physics, Florida State University, Tallahassee, Florida 32306

J.F. Mateja
Argonne National Laboratory, Argonne, Illinois 60439
(Received 6 August 1990)

Sequential decay modes for the four-body final-state reaction, $^{12}C+^{12}C \rightarrow 3\alpha+^{12}C$, are reported at a bombarding energy of 7.5 MeV/u. Position and energy measurement of all three alpha particles allows the kinematic reconstruction of the relative energies of all decay particle combinations. Several known natural parity states are observed from the alpha-particle decay of $^{16}O^*$ and $^{12}C^*$, and in addition unnatural parity states of ^{12}C never before observed in inelastic heavy-ion scattering are seen. The branching fraction for the alpha-particle decay of the 14.08 MeV 4^+ state of ^{12}C to the $^8Be^*$, 2^+ state is measured to be 0.83 ± 0.04. Monte Carlo calculations for the effective solid angle for detection of each process are presented. No evidence is found for any spontaneous three alpha-particle decay of ^{12}C excited states and no previously unknown states are reported.

I. INTRODUCTION

The ^{12}C nucleus is certainly one of the most widely studied nuclides in the entire nuclear chart, yet there are still mysteries about its energy-level structure. Of particular interest to the present investigation is the lack of experimental information on high spin states in ^{12}C. States with $J > 4$ would necessitate the inclusion of $N=2$ or $N=3$ oscillator shell components in the nuclear wave functions, but the presence of such components would not be particularly surprising in view of the large shape distortions known to exist in ^{12}C (Ref. 1).

Prominent model calculations have predicted a number of high spin states[2,3] at excitation energies of ~10 to 35 MeV, although none of them have been observed. The tetrahedral quark structured α-particle model of Robson[2] predicts an extension of the $K=0$ ground-state band to a $J^\pi=6^+$ state near 27 MeV in excitation and a $K=6$ band with $J^\pi=6^+$, 7^+, and 8^+ at Ex ~17, 25, and 34 MeV. Cranked Nilsson model calculations[3] indicate the presence of several bands with high spin components. These bands show the signature splitting into natural and unnatural parity bands, unlike the α-particle model. The Nilsson calculation predicts the ground-state band to terminate at the $J^\pi=4^+$ state, and the well-known 9.64 MeV, 3^- state in ^{12}C becomes a bandhead for 5^- and 7^- states near calculated energies of 18 and 24 MeV. The alpha-particle model also accurately accounts for this state and in addition predicts the band continuation for 4^-, 5^-, and 6^- states which are expected to be near excitation energies of 13, 18, and 24 MeV respectively. Both models are in good agreement on the location of the linear alpha-particle chain band which is a superdeformed band with $\epsilon \sim 1$. The bandhead is the well known $J^\pi=0^+$ state at 7.65 MeV in excitation, followed by $J^\pi=2^+$, 4^+, 6^+, 8^+, and 10^+ members with predicted excitation energies of about 9, 12, 16, 22, and 30 MeV.

Shell-model calculations have been done for ^{12}C (Ref. 4), but the limited space used has not allowed for states with $J > 4$. A number of 4^- states have resulted from the calculations however. The one which lies lowest in excitation energy is at ~13.6 MeV, which is in good agreement with Robson's $J^\pi=4^-$ rotational component of the band built on the octupole, $J^\pi=3^-$, bandhead at $E_x=9.64$ MeV.

Experimental determination of a few of these states would shed considerable light on the applicability of these structure models to light nuclei, however, these high spin band members are very difficult to observe by conventional means. The low Coulomb barrier and α-particle cluster structure practically eliminates γ decay, and the α-particle inclusive spectra will have the α decay of these high excited states superimposed on a prolific energy continuum from $^{12}C^* \rightarrow 3\alpha$ in addition to the characteristic poor energy resolution of heavy-ion inclusive reaction studies.

A study of a somewhat related four-body light-ion reaction, $^{10}B(^3He,p3\alpha)$, has been reported by Waggoner *et al.*[5] Only two of the final-state particles were detected, so spectra still suffered from the continuum background, but careful analysis yielded spin and parity information for many states in ^{12}C. From our point of view other disadvantages of that experiment are its inability to select cluster structures or supply very high incoming angular momentum.

We have initiated a search for previously unknown cluster states in ^{12}C by developing a detection system which takes advantage of the particle decay feature to yield good energy resolution spectroscopy of particle unstable excited states, reduce the interference of the multiparticle decay continuum, and provide angular correlation information on the decay process for possible spin determination of the states. In addition, there is some facility for separating the different possible sequential decay modes which lead to the same multiparticle final state. The method, which is very similar to the one developed by Rae and co-workers at Oxford[6] and Berkeley,[7] is detailed in the following section.

II. EXPERIMENTAL PROCEDURE

The kinematically complete four-body final-state reaction requires that the momenta of three particles be determined as accurately as possible. We accomplish this in the present experiment by measuring position and energy of the three final-state alpha particles. Since much of the decay results in the production of a ^{8}Be(g.s.) particle, we employ a "^{8}Be detector" which has high efficiency for detecting the alpha-particle decay of ^{8}Be(g.s.). Identification of the ^{8}Be(g.s.) reduces the reaction to essentially a three-body final state. The initial general discussion will be in terms of both the three-body and four-body final-state problem and we will revert to strictly a four-body discussion when required by the complexity of the decay. In either case, for particles 1, 2, and 3 or 1, 2, 3, and 4, the last particle numbered is the undetected particle, ^{12}C.

A. Description of method

A schematic diagram for a general detection system for a three-body final state is shown in Fig. 1. The two-body final-state reaction $T(A,B^*)3$ is followed by particle decay of the nucleus $B^* \to 1+2$, and the energy, position, and mass of those two decay products are determined

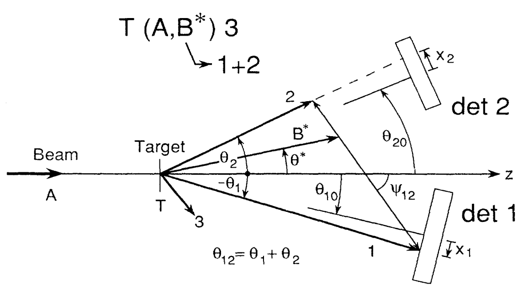

FIG. 1. Schematic of detectors and angle definitions for a general three-body final-state reaction, $T + A \to B^* + 3 \to 1 + 2 + 3$.

by the wide-angle detectors 1 and 2, respectively. Under these conditions the vector momenta of 1 and 2 are known so the momentum of the recoil nucleus, particle 3, is easily calculated. From these the three-body Q value is given by $-Q_3 = E_A - E_1 - E_2 - E_3$. In practice the mass of particle 2, the heavy fragment, is determined by an $E - dE$ counter telescope or by use of a ^{8}Be detector. When the ^{8}Be detector is used, energies and positions of two additional alpha particles are measured and the four-body Q-value equation is given by

$$-Q_4 = E_A - E_1 - E_2 - E_3 - E_4 \; . \tag{1}$$

Peaks in this Q_4 spectrum will indicate the state of excitation of particles 1, 2, 3, and 4. Usually, but not always, the peak with minimum value of $-Q_3$ or $-Q_4$ is selected, which represents all final state particles in their ground states. For any selection of a well separated Q value one can then generate a spectrum of the relative energies of particles i and j by use of the equation

$$\begin{aligned} E_{\rm rel}(ij) &= [1/(M_i + M_j)][E_i M_j + E_j M_i \\ &\qquad - 2\sqrt{E_i E_j M_i M_j} \cos\theta_{ij}] \\ &= E_{i-j} \; . \end{aligned} \tag{2}$$

In the three-body final state, $E_{\rm rel}(12) = E_x(B) + Q_{12}$. After selection of a well defined excited state in B^* from the $E_{\rm rel}$ spectrum, one can generate the two-dimensional angular correlation function $W(\theta^*_{\rm c.m.},\psi)$. Since the energy and momentum of particle 3 have already been determined, one can in addition investigate the relative energy spectra $E_{\rm rel}(13)$ and $E_{\rm rel}(23)$, which, if correlations are present, would describe the sequential reactions $T(A,C^* \to 1+3)2$ and $T(A,D^* \to 2+3)1$, respectively, and for isolated states one can generate the corresponding correlation function. The energy resolution in spectrum $E_{\rm rel}(12)$, that is the relative energy of two directly detected particles, can be quite spectacular for a heavy-ion experiment, especially near the particle decay threshold of B^*. The energy resolution in a $-Q$ spectrum suffers from all the usual degrading effects common to heavy-ion reactions and in the present experiment we observe resolution $\sim$1% of beam energy. Part of the peak width in Q spectra can be attributed to beam energy spread from the LINAC. The relative energy spectra, $E_{\rm rel}(13)$ and $E_{\rm rel}(23)$, in which only one of the two particles being considered is detected directly, have energy resolution somewhat intermediate to the $E_{\rm rel}(12)$ and the Q spectra.

B. Detectors and calibration

The α-particle detector is a 1 cm$\times$ 5 cm position sensitive Si(Li) detector with a depletion depth of $> 700\ \mu$m and with the 5 cm position sensitive direction in the horizontal reaction plane. The ^{8}Be detector is merely two 3000 μm thick alpha detectors mounted with their 5 cm directions parallel and separated by 3.6 mm, and situated symmetrically above and below the reaction plane. The detectors are located typically about 10 cm from the target and are cooled to about −15°C by a circulating alcohol refrigerator.

Position and energy calibrations are done prior to every experiment. Since an aluminum foil is placed over the alpha-particle and ^{8}Be detectors in most cases in order to stop the incident beam, and since the energy signal produced is dependent upon position due to varying charge collection efficiency, the energy calibrations are highly nonlinear. A calibration grid of 21 slit apertures cut in a 0.5-mm-thick Ta mask is placed in front of the 1 cm × 5 cm detectors for calibration and signals from a range of α-particle energies are recorded. In the present case the reaction ^{12}C(^{12}C,α)^{20}Ne is used at bombarding energies of 25 to 45 MeV. The pulse height signals of five alpha-particle groups from each slit, as selected by their position signals, are fit to a function of the form $E = [\alpha(\text{ph})^{1.6} + \beta]^{1/1.6}$, where "ph" designates the pulse height of the energy signal. The coefficients α and β, which determine the energy, are then fit by a fourth-order polynomial in the x position. The typical position resolution [full width at half maximum (FWHM)] along the 5 cm dimension of the detectors is 0.7 mm and results in an angular error of less than ±0.2°.

The effective solid angle of the ^{8}Be detector at the x=0 position, integrated over y, has a maximum value, at $E(^8\text{Be})$=12.5 MeV, of 0.4 msr per mm along the x direction, at a target to detector distance of 105 mm.[8] This value falls off to half maximum at $E(^8\text{Be})$=2.5 and 37.5 MeV for x=0, and at x=±18 mm for $E(^8\text{Be})$=12.5 MeV. The x position of the ^{8}Be particle is determined using conservation of momentum and the reaction plane momentum measurements of both decay α particles.

C. Other experimental details

Self-supporting natural carbon foil targets of areal density ~0.2 mg/cm^2 were bombarded by a 90 MeV ^{12}C beam from the Florida State University Tandem/LINAC. Much thicker targets could be used in this type of measurement without significant loss of energy resolution; however, the experiment is count rate limited at ~30 000 singles events per second with beam currents of only a few tens of nanoamperes. The beam energy is continuously monitored after it traverses the target by measuring the energy of the ^{12}C beam scattered, at ~ 20° from a thin gold secondary target, into a calibrated silicon detector.

The angular settings of detectors are determined by the use of angle encoders which determine the relative angle between detectors, θ_{12} in Eq. (2), to an accuracy of ±0.025°. A beam-line telescope is permanently mounted behind the target chamber for sighting upstream through the chamber to accurately align collimation and antiscattering apertures, and to accurately determine the zero-degree setting for the center of each detector calibration grid. For our geometry the expected error in θ_{12} due to detector position resolution alone is about 0.33°. The largest remaining angular error in θ_{12} results from the uncertainty in the z position of the target. Since $d\theta/dz = \sin\theta/D$, where D is the target to detector distance, errors of greater than 0.1 degrees are easily encountered.

The energy signals from the three detectors are used for establishing the coincidence signal which is used to gate three energy signals, three position signals, and the time-to-amplitude converter (TAC) signal to seven analog-to-digital converters (ADC's) of the data-acquisition system. All seven ADC's must register an event to enable a write command to magnetic tape. The fast coincidence time resolution between the detection of two alpha particles in the ^{8}Be detector, as registered in the TAC, is about 15 ns. The TAC receives a 100 ns gate signal generated by the other α-particle detector. The ratio of true coincidences to accidentals exceeded 10 to 1. True coincidence rates were between 5 and 50 per minute. Calculations of spectra for Eqs. (1) and (2) are done off line; however, the many two dimensional spectra which can be viewed on line include all pair combinations of energy or position for all three detectors.

III. DATA AND DISCUSSION

A. Reactions with final state particles, α, ^{8}Be, and ^{12}C, in their ground states

Data were accumulated for two geometries: (I) $\theta_{20} = -\theta_{10} = 20°$, and (II) $\theta_{20} \sim 15°$, $\theta_{10} \sim 46°$. In each case both detectors subtended about ±12° in the laboratory. Geometry I has large values of θ_{12} and hence emphasizes a higher excitation energy region for ^{12}C decay ($E_x \sim 9$ to 35 MeV) and presents the potential for breakup correlations from an excited ^{12}C near zero degrees. Geometry II emphasizes a lower ^{12}C excitation energy range, ~8.5 to 20 MeV, but also gives a lower event rate from the ^{12}C(^{12}C,^{16}O* → α+^{12}C)^{8}Be reactions since, by detecting the alpha particles at large angles with the ^{8}Be detection on the same side of the beam, the ^{12}C(g.s.) recoil must be on the opposite side of the beam at relatively large angle making for a very large alpha-particle plus ^{12}C breakup angle and correspondingly a very high excitation in ^{16}O.

The alpha-particle coincidence events in the ^{8}Be detector are selected to be ^{8}Be(g.s.) events by using Eq. (2) to calculate the relative energy between the two alpha-particles detected in the ^{8}Be detector. In the resulting spectrum, shown in Fig. 2, the ^{8}Be (g.s.) peak is easily identified. It is clear that there is no apparent production of the ^{8}Be, 2^+, state near 2.9 MeV excitation (relative energy ~3.0 MeV); however, the detection efficiency is greatly diminished at higher relative energies, since by design the maximum efficiency is for the ^{8}Be ground state. The nature and relative magnitude of the continuum at higher relative energies are discussed in Sec. III B. The remainder of spectra discussed in this section have been gated for ^{8}Be in the ground state.

The Q spectrum for final-state particles α, ^{8}Be(g.s.), and ^{12}C generated from coincident events of geometry II,

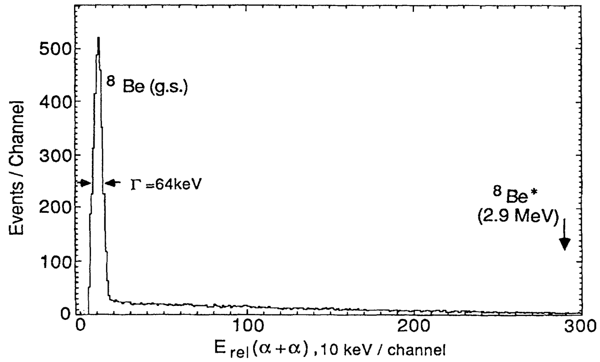

FIG. 2. Relative energy of pairs of alpha particles detected in coincidence in the ^{8}Be detector.

is shown in Fig. 3. The continuum for large negative Q value relative to the ground state peak is a factor of 2 higher for geometry I. Since the ^{8}Be nucleus is already restricted to the ground state by appropriate gating of a Fig. 2 type spectrum, only excited states in ^{12}C show in this spectrum. The ungated four-body Q-spectrum is very nearly the same as Fig. 3, since the two alpha-particles in the ^{8}Be detector will have the same final energies whether or not the decay sequence is through the ^{8}Be $J^\pi=2^+$ excited state or the $J^\pi=0^+$ ground state. There is a little extra background in an ungated Q_4-spectrum arising from greater numbers of accidental coincidences and non-alpha-particle detection.

Three different reactions are possible which can result in these same three final reaction products via sequential binary processes: ^{12}C(^{12}C,^{12}C* $\rightarrow$ α+^{8}Be)^{12}C, ^{12}C(^{12}C,^{16}O* $\rightarrow$ α+^{12}C)^{8}Be, and ^{12}C(^{12}C,^{20}Ne* $\rightarrow$ ^{8}Be+^{12}C)α. For the purpose of discussion in this section we will use the three-body final-state notation referring to these three final state particles, alpha, ^{8}Be(g.s.), and ^{12}C(g.s.), as particles 1, 2, and 3, respectively. For each recorded event the relative energies $E_{\rm rel}(1,2)$, $E_{\rm rel}(1,3)$, and $E_{\rm rel}(2,3)$ are calculated and could correspond to any one of the decays of ^{12}C*, ^{16}O*, or ^{20}Ne*, respectively. A scatter plot of $E_{\rm rel}(1,2)$ versus $E_{\rm rel}(1,3)$ for the data acquired for geometry II is shown in Fig. 4. The vertical and horizontal bands of clustered events correspond to the alpha-particle decay of excited states of ^{12}C and ^{16}O respectively. Events representing ^{8}Be emission from excited states of ^{20}Ne would appear as diagonal bands of negative slope in Fig. 4. Clearly the reaction data are dominated by inelastic scattering and the (^{12}C,^{16}O) reaction, with no evidence for ^{8}Be decay of ^{20}Ne.

Another possibility for the observation of ^{20}Ne* is from the reaction

$$^{12}\mathrm{C} +^{12}\mathrm{C} \rightarrow^{20}\mathrm{Ne}^* + \alpha \rightarrow^{16}\mathrm{O}^* + 2\alpha \rightarrow^{12}\mathrm{C} + 3\alpha \ .$$

This process would produce time and angular correlations between any pair of detected alpha particles and the residual ^{12}C nucleus, but only the last two alpha particles and the residual ^{12}C would be correlated in energy. This is because detection of the first decay alpha particle establishes the momentum of ^{20}Ne*, therefore the resulting ^{12}C+2α will have the c.m. velocity of the ^{20}Ne* and the energy relative to the c.m. equal to the decay energy of ^{20}Ne* $\rightarrow$^{12}C+2α. Scatter plots of the relative energy

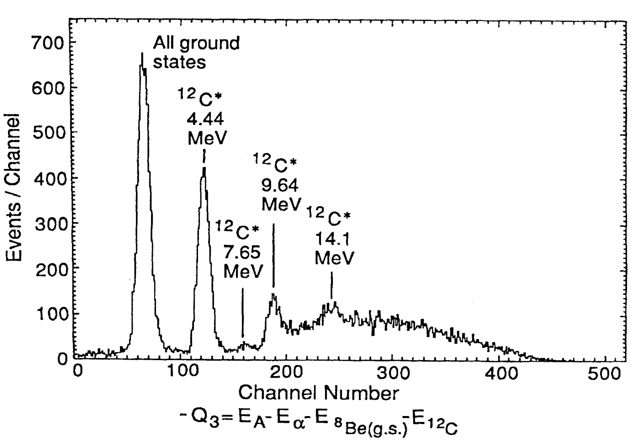

FIG. 3. The Q spectrum generated by use of Eq. (1) for the reaction ^{12}C+^{12}C$\rightarrow$ α+^{8}Be(g.s.)+^{12}C* and for geometry II, $\theta_{\alpha 0} = \theta_{10} \simeq 46°$, $\theta_{^8{\rm Be}_0} = \theta_{20} \simeq 15°$. Only events for ^{8}Be in the ground state as determined from Fig. 2 are included. Calibration is 80 keV/channel.

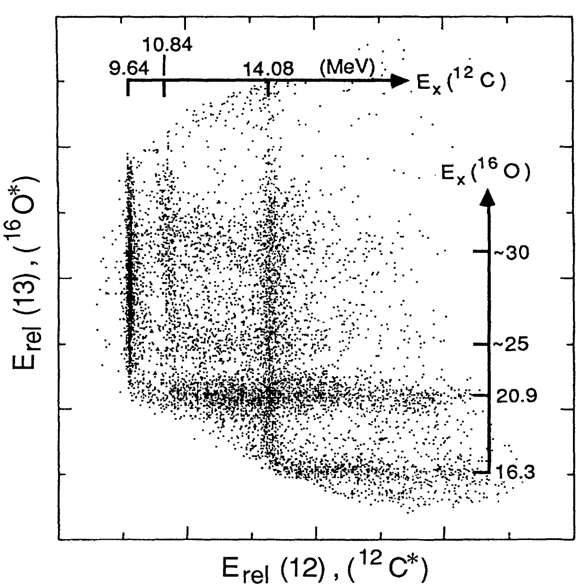

FIG. 4. Scatter plot spectrum, $E_{\rm rel}(12)$ vs $E_{\rm rel}(13)$, for geometry II, $\theta_{10} \simeq 46°$, $\theta_{20} \simeq 15°$, gated for ^{8}Be(g.s.) and ^{12}C(g.s.).

of pairs of alpha particles and the residual ^{12}C versus total kinetic energy of all three alpha particles relative to their center of mass have been formed and no correlations which could be attributed to states in ^{20}Ne have been found. The effective solid angles for detection of these ^{20}Ne* decay processes are ~0.2 msr for ^{8}Be(g.s.) emission and about an order of magnitude less for the sequential 2α decay. Both values are for $E_x(^{20}\mathrm{Ne}) \sim 20$ to 30 MeV. See Ref. 9 for details.

The two dimensional event spectrum of Fig. 4 illustrates the degree of inseparability of the reactions $^{12}C(^{12}C,^{12}C^* \to \alpha+^{8}Be)^{12}C$ and $^{12}C(^{12}C,^{16}O^* \to \alpha +^{12}C)^{8}Be$. The generation of relative energy spectra without regard to the overlap of these reactions in our detector space would lead to unneccesarily high background. The decay energy spectra from these reactions, shown in Fig. 5, are projected from the data of Fig. 4 with gating to partially separate the reactions. In the decay spectrum of Fig. 5(a), ^{12}C decay, we have projected only those events of Fig. 4 above the 20.9 MeV region in ^{16}O excitation. No previously unknown excited states of ^{12}C are apparent in Fig. 5(a) up to an excitation energy of 19 MeV, although it should be noted that the relative coincidence detection efficiency diminishes significantly at high excitation. The states observed in ^{12}C* decay at 9.64, 10.84, and 14.08 MeV are the only known T=0 natural parity states with unambiguous spin assignments in ^{12}C for excitations above the first unbound state at 7.65 MeV.[1] There is no evidence in our data for the superdeformed band of states with $J^\pi=2^+$, 4^+, and 6^+ predicted[2,3] at E_x ~9, 12, and 16 MeV or the $J^\pi=5^-$ state at E_x ~18 MeV.[2,3]

The ^{16}O* spectrum, $E_{\rm rel}(13)$ in Fig. 5(b), has been projected from Fig. 4 by first eliminating the strong vertical bands which correspond to the decay of ^{12}C* states near 9.6 and 14.1 MeV in excitation. In addition to the known $J^\pi=6^+$ and 7^- states in ^{16}O at E_x=16.28 and 20.28 MeV, respectively, we also observe two higher energy regions of excitation near 25 and 30 MeV. This spectrum is similar to that observed by Rae *et al.*[10], who have determined the 30 MeV structure to be a coherent mixture of $J^\pi=8^+$ and 9^-.

In geometry I, the reaction angle of the product nucleus ^{12}C* is in the vicinity of zero degrees and the detector angle centers are 40° apart. This geometry provides for the observation of alpha-particle decay of excited states in ^{12}C nearly up to 40 MeV and for a simplified decay correlation, since the small angle of ^{12}C* approximates the geometry of method II of Litherland and Ferguson[11] and the conditions set by Rae *et al.*[6] Unfortunately, as we shall see this forward-angle geometry also greatly increases the frequency of background events from all causes.

To form the spectrum $E_{\rm rel}(12)$, peaks in which will represent excited states of ^{12}C, we again select ^{8}Be(g.s.) and ^{12}C(g.s.) events from spectra similar to Figs. 2 and 3, and gate out all events which would correspond to ^{16}O excitations at $\leq$20.9 MeV in a scatter plot similar to Fig. 4. The resulting $E_{\rm rel}(12)$ spectrum is shown in Fig. 6. Again only a few known excited states of ^{12}C are apparent up to a possible excitation energy of ~32 MeV. The

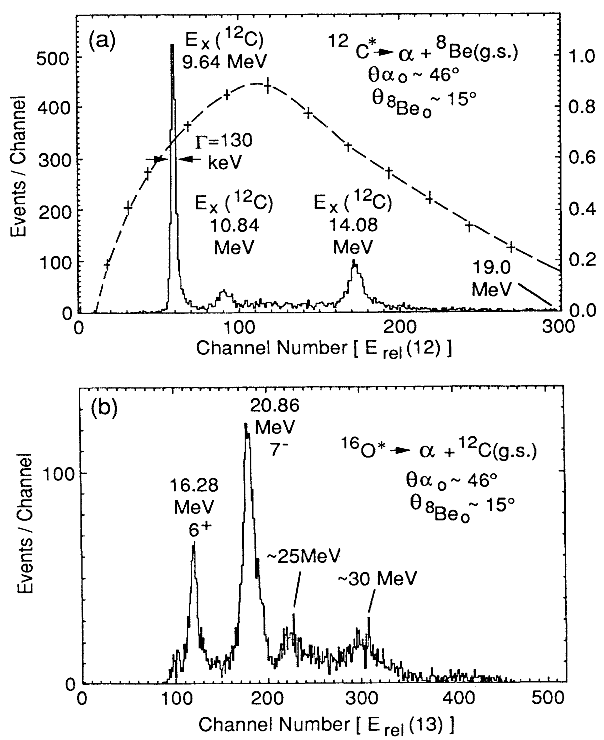

FIG. 5. Relative energy spectra as gated projections from Fig. 4, (a) ^{12}C* decay spectrum with 40 keV/channel, with the dashed curve describing the energy dependence of the effective solid angle. (b) ^{16}O* decay spectrum with 80 keV/channel. See text for gates on Fig. 4 data.

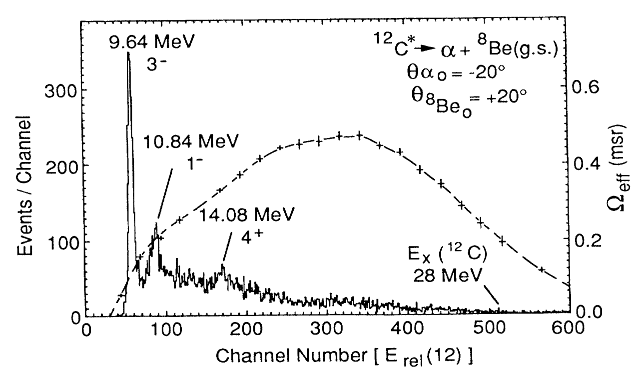

FIG. 6. Relative energy spectrum for $^{12}C^* \to \alpha+^{8}Be(g.s.)$ for geometry I, $\theta_{10} = -20°$ and $\theta_{20}=20°$. Calibration is 40 keV/channel. The dashed curve describes the energy dependence of the effective solid angle.

increased background in this spectrum is probably due to an increased accidental coincidence rate at this smaller $\theta_{\alpha 0}$ and true coincidence involving ^{12}C nuclei penetrating the aluminum absorber foil placed in front of the alpha-particle detector. (Note that the greatly reduced ^{12}C energy is in the range of detected alpha-particle energies making it indistinguishable from an alpha particle.) The $E_{\rm rel}(13)$ spectrum,[9] not shown for geometry I, illustrates prominently the alpha-particle decay of ^{16}O* states at $E_x \simeq 10.36$ and 14.62 MeV in addition to those seen in Fig. 5(b) at 16.28 and 20.86 MeV.

Rae has shown for sequential breakup reactions resulting in spin zero particles that the angular correlation function, W($\theta^*_{\rm c.m.},\psi$), in the neighborhood of zero degrees, will have maxima and minima which trace lines in $\theta^*_{\rm c.m.},\psi$ space which have slopes which are proportional to the angular momentum of the particle-decaying excited state.[6,12] Application of this technique in the present case is therefore restricted to the geometry I spectrum of Fig. 6 and only the ^{12}C excited states at 9.64 and 10.84 MeV have sufficient yield. In spite of a peak to background ratio of ~1/1 for the 10.84 MeV state, the ridges of maxima in the yield, Y(θ^*,ψ), are clearly evident[9] for both states and their slopes have a ratio of 3/1 in agreement with the spin assignments for these states.

This method has been applied to ^{12}C + ^{12}C twice previously to investigate the α + ^{8}Be(g.s.) + ^{12}C exit channels, once by Rae *et al.*,[10] at 110 MeV as already mentioned, and recently by Shimoura *et al.*,[13] at $E(^{12}\text{C})$=90, 110, and 140 MeV. In both cases the final state particles detected in coincidence were ^{12}C and an alpha particle which leads to poorer-quality Q spectra since the ^{8}Be(g.s.) cannot be uniquely identified. Good results are achieved for ^{16}O* $\rightarrow \alpha$ + ^{12}C; however, the relative energy spectrum for ^{12}C* $\rightarrow \alpha$ + ^{8}Be(g.s.) shown in Shimoura's work has much higher background than in our Fig. 5(a) and they fail to observe the 10.84 MeV, $J^\pi=1^-$ state of ^{12}C, clearly demonstrating the sensitivity of the present method. Equally important for studying ^{12}C* decay is that the ^{12}C + α detection method of Shimoura[13] and Rae[10] is not sensitive to ^{8}Be*, therefore the decay channels of ^{12}C* $\rightarrow \alpha$ + ^{8}Be*(2.9 MeV), reported in the next section, are undetectable.

B. Reactions with a $J^\pi=2^+$ final-state particle

All of the data and discussions of this subsection pertain to the geometry II detector configuration. Of the three 1 cm × 5 cm alpha-particle detectors, detector 1 is centered at 46° from the beam and detectors 2 and 3, above and below the reaction plane are centered at $\theta=15°$, $\phi=\pm 3.7°$. Four-body notation is used with particle 4 being the undetected residual ^{12}C nucleus, and each alpha particle is numbered according to the number designating the detector in which it registers.

The reactions ^{12}C + ^{12}C $\rightarrow 3\alpha$ + ^{12}C* are easily identified in the Q spectrum of Fig. 3. The events with residual ^{12}C nuclei in the $J^\pi=2^+$ state at E_x=4.44 MeV can be selected and the relative energy between the three detected alpha-particles, $E_{1\text{-}2\text{-}3}$, can be calculated. The resulting histogram contains the yields of all alpha-particle decaying ^{12}C states regardless of the decay channel, but it contains no ^{12}C states not observed in ^{12}C $\rightarrow \alpha$ + ^{8}Be(g.s.), Fig. 5(a).

A more interesting final state system is α+^{8}Be*(2$^+$) + ^{12}C(g.s.) where the α+^{8}Be*(2$^+$) has resulted from the particle decay of an inelastically scattered ^{12}C nucleus. The decay via alpha-particle emission of ^{12}C* in the 9.63 MeV (3$^-$) and 10.84 MeV (1$^-$) excited states to the first excited state of ^{8}Be would be greatly inhibited from both energy and angular momentum considerations. The decay of the 14.08 MeV excited state of ^{12}C through ^{8}Be* (2.9 MeV) would be much more probable; however, alpha-particles from the subsequent decay of ^{8}Be* emerge within a cone of full angle ~30°. There is therefore a very low probability of ^{8}Be* detection in the "^{8}Be detector," pair combination 2-3, and a much higher probability for detection in detector pairs 1-3 and 1-2. The effective solid angle for ^{8}Be* detection has been calculated for this reaction and our detector geometry and the results are shown in Fig. 7. Over the excitation energy range of the broad first excited state of ^{8}Be the effective solid angle for detection by use of any pair of alpha-particle detectors, curve (a), is about four times that of detector pair 2 and 3, curve (b).

In order to separate ^{8}Be(g.s.) events from ^{8}Be* events we can still investigate the $E_{2\text{-}3}$ spectrum where the ^{8}Be(g.s.) events are clearly identifiable (see Fig. 2). Which ^{12}C* states decay to the ^{8}Be* (2.9 MeV) state becomes evident when we form the event scatter plot (Fig. 8) of $E_{2\text{-}3}$ versus $E_{1\text{-}2\text{-}3}$. This is the relative en-

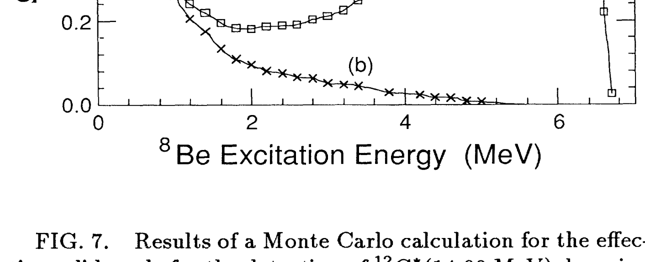

FIG. 7. Results of a Monte Carlo calculation for the effective solid angle for the detection of ^{12}C*(14.08 MeV) decaying to α+^{8}Be, vs the ^{8}Be excitation energy. Detectors are in geometry II, $\theta_{10} \simeq 46°$, $\theta_{20} \simeq 15°$. Curve (a) is for the primary alpha particle detected in any detector. Curve (b) is for the primary alpha particle detected in detector 1.

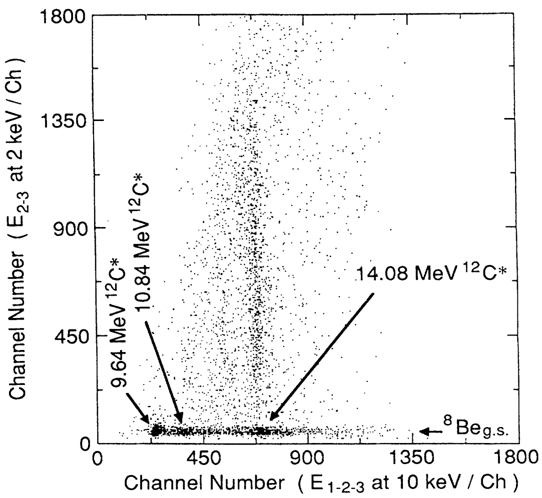

FIG. 8. Scatter plot of $E_{2\text{-}3}$, the relative energy of alpha particles detected in the "^{8}Be-detector," vs $E_{1\text{-}2\text{-}3}$, the total energy of all three alpha particles relative to their center of mass. The vertical band of events at $E_x(^{12}C)=14.08$ MeV above ^{8}Be(g.s.) events represents the decay $^{12}C^*(14.08$ MeV) $\to \alpha + {}^8Be^*(2.9$ MeV). The events are for $E_{1\text{-}4} > 14.5$ MeV.

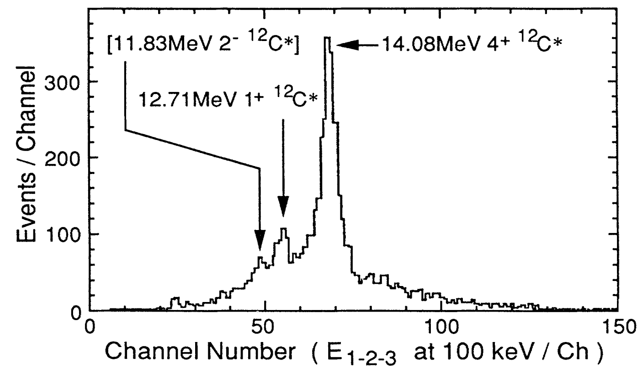

FIG. 9. Relative energy, $E_{1\text{-}2\text{-}3}$, spectrum of events of Fig. 8 for which $E_{2\text{-}3} \geq 200$ keV. $E_{1\text{-}2\text{-}3}$ is the total energy of all three detected alpha particles relative to their center of mass. Excited states of ^{12}C which decay to $\alpha + {}^8Be^*(2.9$ MeV) are indicated.

ergy of the alpha particles detected in the ^{8}Be-detector versus the total energy of all three alpha particles relative to their center of mass, in this case the center of mass of the decaying $^{12}C^*$ nucleus. The band of events at $E_x(^{12}C) \simeq 14.08$ MeV which extend over a broad range in $E_{2\text{-}3}$ above the ^{8}Be(g.s.) indicates the decay of $^{12}C^*$ (14.08 MeV) to $^8Be^*$ and shows that that transition overwhelmingly dominates the $^8Be^*$ events.

It is noted in Fig. 8 that the center of the distribution of events in this band is not near $E_{2\text{-}3} \sim 3$ MeV as might be expected since $^8Be^*(2^+)$ has a decay energy of ~ 3 MeV, rather the $E_{2\text{-}3}$ distribution centers at about half that value. This shift is not due to the energy dependence of the effective solid angle, Fig. 7, curve (b). It is because $E_{2\text{-}3}$ represents the decay energy of $^8Be^*(2^+)$ only when alpha particles 2 and 3 are from that $^8Be^*$ decay and Fig. 7 shows that $\frac{3}{4}$ of the $^8Be^*$ events are not detected in that manner. Most of the events in the $^8Be^*$ band in Fig. 8 are the result of one of the $^8Be^*$ decay alpha particles being detected in detectors 2 or 3 and the other in detector 1. The actual energy and width of the $^8Be^*(J^\pi=2^+)$ state can be extracted[9] from a scatter plot of $E_{1\text{-}3}$ versus $E_{1\text{-}2}$ and it yields $E_x=2.90\pm0.05$ MeV and $\Gamma=1500\pm100$ keV in good agreement with tabulated values.[1]

Although the band of events in Fig. 8 near $E_x(^{12}C)=14.08$ MeV and for $E_{2\text{-}3} \geq 200$ keV does not represent the actual line shape of $^8Be^*$ (2.9 MeV), the total number of these events is still representative of the transitions $^{12}C^*(14.08$ MeV) $\to \alpha + {}^8Be^*(2.9$ MeV). In Fig. 9 we present a histogram of the sum of all events of Fig. 8 for $E_{2\text{-}3} \geq 200$ keV versus $E_{1\text{-}2\text{-}3}$, revealing additional alpha-particle transitions to $^8Be^*(2.9$ MeV) from the unnatural parity ^{12}C states at $E_x \simeq 11.83$ and 12.71 MeV. Also there are yield indications near channel numbers 23 and 37 which could correspond to $E_x(^{12}C)=9.64$ and 10.83 MeV; however, the yield at 9.64 MeV is merely feedthrough from gating out the ^{8}Be(g.s.) events in Fig. 8 and the 10.83 MeV yield is too small to be statistically significant.

The information at hand now allows us to extract a branching fraction, $\Gamma_{\alpha 1}/(\Gamma_{\alpha 0}+\Gamma_{\alpha 1})$, for the alpha-particle decay of the 14.08 MeV state of ^{12}C. A chi-squared fitting routine has been used to describe the histograms of Figs. 5(a) and 9 as a quadratic background plus Gaussian line shapes for the three transitions indicated in each. The extracted yields for $^{12}C^*(14.08$ MeV) $\to \alpha + {}^8Be(g.s.)$ and for $^{12}C^*(14.08$ MeV) $\to \alpha + {}^8Be^*(2.9$ MeV) have errors of 6.0% and 4.1%, respectively, while the errors in the corresponding Monte Carlo calculated effective solid angles are 1.7% and 4.2%, respectively. The result is a branching fraction to $^8Be^*$ of 0.83 ± 0.01, which is equal to $\Gamma_{\alpha 1}/\Gamma$, since we find no evidence for spontaneous 3α decay. The accuracy of this value depends on the degree to which the angular correlation function, $W(\theta^*_{c.m.},\psi)$, is integrated to its average value by the finite detector geometry since isotropy is assumed in the Monte Carlo calculations of the effective solid angles. From scatter plots in $(\theta^*_{c.m.},\psi)$ space we find that the $\theta^*_{c.m.}$ range is $\sim 30°$ to $65°$ for both transitions so that that variable should not introduce additional error. Also for the ground state transition, $\Delta\psi \sim 50°$ with ψ limits $\sim 90°$ and $160°$ and there is no significant structure in the two dimensional scatter plot. This is similar to the result of Rae *et al.*[6] who found the decay correlation function following inelastic ^{18}O scattering to be washed out for large reaction angles. The ψ dependence of $\alpha + {}^8Be^*$ correlation cannot be determined directly from the data due to our inability to determine which alpha particle constitutes the primary decay. The range of ψ detected is known from Monte Carlo calculations to be 120° and there is no apparent oscillatory behavior in the correlation for any assumed primary decay. Even if one assumes that our integration of the correlation functions is in error from the average value by 20% for each transition, the branching fraction is still fairly accurate, given by $\Gamma_{\alpha 1}/\Gamma=0.83\pm0.04$.

In the work of Waggoner *et al.*[5] on the $^{10}B(^{3}He,p\alpha\alpha\alpha)$ reaction a branching fraction Γ_0/Γ was determined, ignoring the effective solid angle difference, to range from 0.11 to 0.38 for various angle combinations of a p-α coincidence measurement, which is still consistent with our angle integrated result. McKeown and Garvey[14] have performed a Litherland and Ferguson, method II, experiment in the reaction $^{12}C(\alpha,\alpha')^{12}C^* \rightarrow \alpha_0 + {}^{8}Be(g.s.)$ and obtain a value of $\Gamma_{\alpha 0}/\Gamma=0.09\pm0.03$. This ground state decay width together with our value of $\Gamma_{\alpha 0}/(\Gamma_{\alpha 0}+\Gamma_{\alpha 1}) = 0.83 \pm 0.04$ would require a spontaneous 3α decay width of $^{12}C^*$(14.08 MeV) of more than five times Γ_0, which is inconsistent with the 3α-contribution measurements of Waggoner[5] and the current work. A semiclassical estimate[15] is very close to our measurement, yielding a value of $\Gamma_{\alpha 1}/\Gamma=0.8$. A more detailed theoretical calculation is under way.[16]

ACKNOWLEDGMENTS

The authors wish to acknowledge the many fruitful discussions with Dr. W.D.M. Rae and Dr. D. Robson and the generously shared LINAC expertise of Dr. E.G. Myers, Dr. A.D. Frawley, and Dr. J.D. Fox. The assistance during the early stages of this work of Amy Toppins and Ken Lamkin is gratefully appreciated. This work was supported by the State of Florida and the National Science Foundation.

[1] F. Ajzenberg-Selove, Nucl. Phys. **A433**, 1 (1985).
[2] D. Robson, Nucl. Phys. **A308**, 381 (1978).
[3] I. Ragnarsson, S. Aberg, H.-B. Hakansson, and R.K. Sheline, Nucl. Phys. **A361**, 1 (1981).
[4] R.S. Hicks, J.B. Flanz, R.A. Lindgren, G.A. Peterson, L.W. Fagg, and D.J. Millener, Phys. Rev. C **30**, 1 (1984); D.J. Millener and D. Kurath, Nucl. Phys. **A255**, 315 (1975).
[5] M.A. Waggoner, J.E. Etter, H.D. Holmgren, and C. Moazed, Nucl. Phys. **88**, 81 (1966).
[6] W.D.M. Rae and R.K. Bhowmik, Nucl Phys. **A420**, 320 (1984); R.K. Bhowmik and W.D.M. Rae, Phys. Lett. **136B**, 149 (1984); S. March and W.D.M. Rae, *ibid.* **153B**, 21 (1985).
[7] W.D.M. Rae, A.J. Cole, A. Dacal, R. Legrain, B.G. Harvey, J. Mahoney, M.J. Murphy, R.G. Stokstad, and I. Tserruya, Phys. Lett. **105B**, 417 (1981); W.D.M. Rae, A.J. Cole, B.G. Harvey, and R.G. Stokstad, Phys. Rev. C **30**, 158 (1984).
[8] Florida State University Superconducting Accelerator Laboratory Progress Report, 1986–1988, pp. 70–85.
[9] David D. Caussyn, Ph.D. dissertation, Florida State University, 1990 (unpublished).
[10] W.D.M. Rae, S.C. Allcock, S. Marsh, and B.R. Fulton, Phys. Lett. **156B**, 167 (1985).
[11] A.E. Litherland and A.J. Ferguson, Can. J. Phys. **39**, 788 (1961).
[12] A.E. Smith, S.C. Allcock, W.D.M. Rae, B.R. Fulton, and D.W. Banes, Nucl. Phys. **A441**, 701 (1985); W.D.M. Rae, P.R. Keeling, and S.C. Allcock, Phys. Lett. **184B**, 133 (1987).
[13] S. Shimoura, A. Sakaguchi, T. Shimoda, T. Fukuda, K. Ogura, K. Katori, and H. Ogata, Nucl. Phys. **A452**, 123 (1986).
[14] R. McKeown and G.T. Garvey, Phys. Rev. C **16**, 482 (1977).
[15] D. Robson (private communication).
[16] D.D. Caussyn and D. Robson (unpublished).